photonics

MDPI

Article

Optical Encryption Based on Cascaded and Multi-Images Integrated Liquid Crystal Elements with High Security

Ying Ma [1,*], Haonan Li [1], Yongning Cheng [1] and Yuechu Cheng [2]

[1] Key Laboratory of Light Field Manipulation and Information Acquisition, Ministry of Industry and Information Technology, School of Physics Science and Technology, Northwestern Polytechnical University, Xi'an 710129, China; hnli@nwpu.edu.cn (H.L.); yncheng@mail.nwpu.edu.cn (Y.C.)

[2] State Key Laboratory (SKL) on Advanced Displays and Optoelectronics Technologies, Department of Electronic and Computer Engineering, Hong Kong University of Science and Technology, Clear Water Bay, Kowloon 999077, Hong Kong; ychengbv@connect.ust.hk

* Correspondence: maying916@nwpu.edu.cn

Abstract

We propose and demonstrate an optical encryption scheme based on cascaded photo-aligned liquid crystal (LC) elements with single-to-multi-image integration. Unlike conventional approaches relying on far-field holography, the proposed method utilizes near-field modulation to improve image capacitance. Theoretical analysis based on a modified Malus's law provides several optimized orientation-angle distribution phases for optical encryption and decryption with single- or multi-image integrated into the encrypted phase. By employing these phases as LC orientation-angle distributions, corresponding LC elements were fabricated using our single-step exposure photoalignment system. Several independent target images can be reconstructed under different decrypted phases of the second LC element. Both simulations and experiments validate that the proposed scheme achieves a high quality of image reconstruction up to four integrated images. Furthermore, the impacts of LC phase mismatch and spatial misalignment were also investigated, showing that only small mistakes of phases (<20%) and positions (<0.08 mm, <0.2°) can lead to successful image reconstruction, making the system more secure. This work provides a framework for higher-capacity optical encryption and advanced photonic information processing.

Keywords: liquid crystal optical encryption; multiple images; near-field image display; information security

1. Introduction

The rapid advancement of information technology has made data security and intellectual property protection critical global concerns. Traditional data encryption techniques face slow processing speeds and high computational complexity, particularly when managing large-scale image and video data. Optical encryption has gained more attention for its speed, parallel processing capabilities, and ability to encrypt multidimensional data. This technology uses light's properties—such as phase, amplitude, and polarization—to efficiently conceal and transmit information [1,2]. The traditional double-random phase encoding (DRPE) system randomizes input information in both spatial and frequency domains, improving security [3,4]. Traditional optical encryption methods depend on interference and diffraction techniques [5–7], which are challenged by large design sizes, making them unsuitable for compact, miniaturized devices. In this context, metasurface encryption

Check for updates

Received: 3 June 2026
Revised: 23 June 2026
Accepted: 29 June 2026
Published: 30 June 2026

Copyright: © 2026 by the authors. Licensee MDPI, Basel, Switzerland. This article is an open access article distributed under the terms and conditions of the Creative Commons Attribution (CC BY) license.

is an emerging technology that uses the distinctive optical properties of metasurfaces to ensure secure information transmission and storage. Multiplexed metasurfaces, which rely on factors such as illumination angle, polarization, and orbital angular momentum, have gained much interest [8–13], although faced with high cost, nanoscale fabrication processes, and formidable challenges.

Liquid crystals (LCs), with anisotropic molecular structures, are important birefringent materials that offer multi-dimensional modulation, voltage sensitivity, and high diffraction efficiency [14,15]. The advancement of photoalignment technology allows for the alignment of complex patterns, creating pixel-level programmable alignments that present new opportunities for optical encryption applications [16–18]. In comparison to metasurfaces, LCs provide advantages such as adjustable optical responses, reconfigurable orientation, low cost, high birefringence, and transparency, further enhancing their potential in optical applications. Planar optical elements made from LCs have shown strong potential in optical encryption due to their compact structure, low fabrication cost, and efficient light field modulation capability [19–23]. Compared with conventional single-layer LC encryption systems, cascaded LC structures provide additional degrees of freedom through the interaction between multiple LC layers, thereby enabling multidimensional multiplexing based on parameters such as polarization, rotation angle, and propagation distance. However, current LC cascaded encryption systems still face several challenges. Alignment accuracy and optical system configuration have a great influence on reconstruction quality, while increasing the number of multiplexing channels may introduce inter-channel crosstalk and higher optimization complexity [24,25].

Although optical encryption has demonstrated promising performance, information leakage remains a concern when the encrypted data is encoded onto a single element or when only one decryption channel is required. Therefore, there is an urgent need for an optical encryption approach that can simultaneously provide enhanced security and direct imaging capabilities. In this work, we introduce an optical encryption method using polarization-based binary encoding. Multiple chaotic sequences scramble the pixel values of the original image, and when the LC cell meets the half-wave condition, different pixel values produce exit light with varying polarization states. To strengthen security, we propose a separate encryption information strategy, enabling decryption through a cascading method. With the cascading method, obtaining a single LC element reveals no useful information; instead, only certain polarized lights and several correct LC elements can work together for successful decryption. Furthermore, multiple target images are integrated into a single encrypted phase, thereby enhancing the information capacity of the system. In addition, the security performance of the proposed scheme is systematically evaluated by analyzing phase mismatch and spatial misalignment during the decryption process. This work validates the feasibility of the scheme both theoretically and experimentally, demonstrating the successful decryption of integrated images.

2. Theory

The light modulation by anisotropic LC molecules can be described using the Jones matrix. Assuming the angle between the long axis of the LC molecules and the horizontal direction is θ_1, the Jones matrix can be expressed as

$$J_1 = \mathrm{R}(-\theta) J_0 \mathrm{R}(\theta) = \begin{bmatrix} \cos\theta_1 & -\sin\theta_1 \\ \sin\theta_1 & \cos\theta_1 \end{bmatrix} \begin{bmatrix} \mathrm{e}^{\mathrm{i}\Gamma} & 0 \\ 0 & \mathrm{e}^{-\mathrm{i}\Gamma} \end{bmatrix} \begin{bmatrix} \cos\theta_1 & \sin\theta_1 \\ -\sin\theta_1 & \cos\theta_1 \end{bmatrix} \quad (1)$$

where R(θ) denotes the rotation matrix, and Γ is the phase delay between the ordinary (o) and extraordinary (e) rays in the LC, which is given by

$$\Gamma = \frac{2\pi(n_e - n_o)d}{\lambda} \tag{2}$$

where n_o and n_e are the refractive indices of the LC for the ordinary and extraordinary rays, respectively, λ is the wavelength of the incident light, and d is the thickness of the LC layer. The half-wave condition ($\Gamma = 180^\circ$) for a specific wavelength can be met by adjusting the thickness d. When horizontally polarized light passes through the LC layer (with thickness d satisfying the half-wave condition), the Jones vector of the transmitted light is expressed as

$$\begin{bmatrix} E_x \\ E_y \end{bmatrix} = J_1 \begin{bmatrix} 1 \\ 0 \end{bmatrix} = \begin{bmatrix} \cos(2\theta_1) & \sin(2\theta_1) \\ \sin(2\theta_1) & -\cos(2\theta_1) \end{bmatrix} \begin{bmatrix} 1 \\ 0 \end{bmatrix} = \begin{bmatrix} \cos(2\theta_1) \\ \sin(2\theta_1) \end{bmatrix} \tag{3}$$

A decryption phase key consists of a phase value array corresponding to the encryption phase. This key counteracts the phase distortion introduced by the encryption phase, allowing the encrypted information to be recovered. The encrypted information is revealed under the influence of a polarizer, and this process can be analyzed using the Jones matrix:

$$\begin{bmatrix} E_{xout} \\ E_{yout} \end{bmatrix} = \begin{bmatrix} 0 & 0 \\ 0 & 1 \end{bmatrix} J_2 \begin{bmatrix} E_x \\ E_y \end{bmatrix} = \begin{bmatrix} 0 \\ \sin[2(\theta_2 - \theta_1)] \end{bmatrix} \tag{4}$$

$$I_{out} = I_0 \sin^2[2(\theta_2 - \theta_1)] \tag{5}$$

where θ_2 represents the angle between the long axis of the LC molecules in the decryption phase and the horizontal direction. $\begin{bmatrix} 0 & 0 \\ 0 & 1 \end{bmatrix}$ is the Jones matrix of the polarizer, signifying that its transmission axis is aligned with the y-axis. J_2 represents the Jones matrix of the second LC element. After passing through two LC cells with thicknesses satisfying the half-wave condition, the horizontally polarized light remains linearly polarized, but its polarization direction is determined by θ_1 and θ_2. When the thickness of the LC layer meets the half-wave condition, the direction of the LC molecular orientation vector corresponds to the fast axis of the half-wave plate. By controlling the distribution of the LC molecular orientation vectors in each small region, we can generate linearly polarized light with varying polarization states.

The encrypted information is divided into two-phase matrices: the binary encryption phase, generated through random scrambling, and the binary decryption phase, obtained by adding the original image to the encryption phase. A binary image is used to illustrate the process of obtaining the decryption phase, but the method is not limited to binary image encryption. Figure 1a, 1b and 1c present the pixel values of the original image, encryption phase, and decryption phase, respectively. As the original image and encryption phase contain only two values, 0 and 1, their sum results in three possible values: 0, 1, and 2. The sum produces an image that is no longer binary, which may affect the orientation angle of the LC molecules. For pixel values greater than or equal to 2, 2 is subtracted to ensure the decryption phase remains a binary image. In Figure 1d, a value of 0 in the encryption phase and decryption phase corresponds to an LC molecular orientation angle of 0°, while a value of 1 indicates an orientation angle of 45°. This enables the adjustment of the outgoing light's polarization state to accurately reveal the original image information.

Simulation results are shown in Figure 2. When the incident beam is modulated by the encryption phase and directed onto an LC sample with the appropriate binary decryption

phase, the correct pattern displaying the word "NPU" is revealed in Figure 2a. Figure 2b,c illustrates the image information when the binary encryption and binary decryption phases do not align. Only a beam of light carrying no valid information is obtained, which, in terms of spatial averaging, resembles natural light.

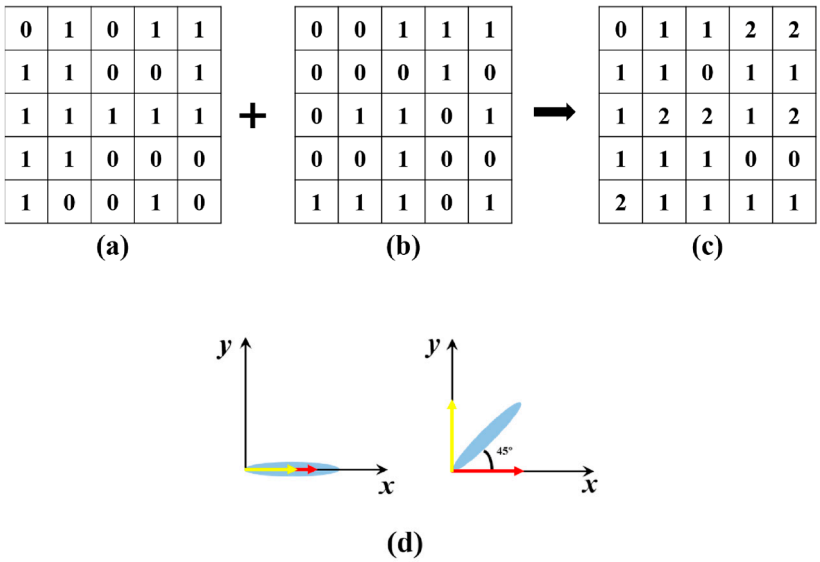


Figure 1. Schematic diagram of the cascaded encryption principle. (**a**) Partial pixel values of the target image; (**b**) partial pixel values of the encrypted image; (**c**) pixel values of the decrypted image; (**d**) relationship between the orientation of liquid crystal molecules and the incident and emergent light (red represents incident light, yellow represents emergent light).

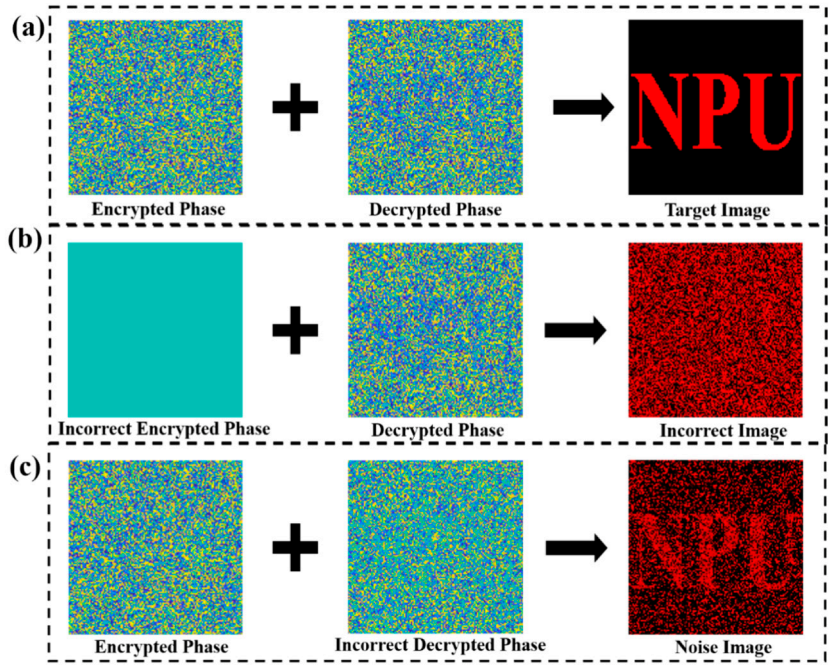


Figure 2. Schematic diagram of simulated decryption: (**a**) the target image when the binary encryption phase matches the binary decryption phase; (**b**) incorrect image when the encryption phase is completely incorrect; (**c**) the noisy image when the decryption phase is partially incorrect.

3. Fabrications and Results

The experiments were carried out in a laboratory with a constant temperature of 26 °C and a relative humidity of about 30%. The fabrication processes of the LC elements mainly include: ozone treatment (to enhance the hydrophilicity of the substrate surface),

spin-coating of the SD1 (a sulfonic azo dye) alignment layer with 3000 r/s for 30 s, drying substrates for 15 min, photoalignment using exposure system for 15 min, and spin-coating of the liquid crystal polymer (OCM-A0, 30%, Raitomaterials, China) with precoating 800 r/s for 5 s and 2650 r/s for 30 s (followed by UV curing for 30 s). A0 has birefringence of n_o = 1.526 and n_e = 1.675 at 633 nm. The thickness was set to approximately 2.12 μm to meet the half-wave condition. The details for a single-step exposure system consisting of a light source, a Glan–Taylor prism (GTP), a beam expander (BE), a lens, a planar mirror, a half-wave plate (HWP), a right-angle prism (RAP), a spatial light modulator (SLM), and a quarter-wave plate (QWP). The light source is a fiber laser with a working wavelength of 450 nm, providing both a wavelength suitable for the alignment layer response and stable energy for the system. Different grayscale images are loaded onto the spatial light modulator to achieve different orientations of the LC molecule [26]. The exposure system has a resolution of 7 μm and 2 μm m according to the size of the light spot. And in our experiment, a resolution of 7 μm was used. Since the optimization algorithm operates on the pixel level, the underlying principle remains essentially the same for fabrication resolutions of 2 μm and 7 μm. In this study, a resolution of 7 μm was adopted primarily to facilitate a more direct validation of the theoretical simulation. The binary encryption and decryption phases have phase pixel arrays of size 900 × 900. The photos that loaded into the SLM for photoaligning LC molecules are generated by encrypted and decrypted phase patterns calculated by Equations (1)–(5). The fabricated LC cell has an overall size of 2 mm × 2 mm, while the effective patterned region of the 2D-LCPG is 6300 μm × 6300 μm. In the experiments, a minimum unit of 9 × 9 pixels was adopted, so the alignment tolerance is approximately ±31.5 μm.

Figure 3 shows the optical encryption system, where the decryption process is achieved by aligning the encryption LC cell with the decryption LC cell in space. The laser beam was linearly polarized parallel to the *x*-axis and the polarizer placed before the CCD was set to have the polarization in the *z*-axis. The CCD was used to capture reconstructed images by placing a polarizer in front.

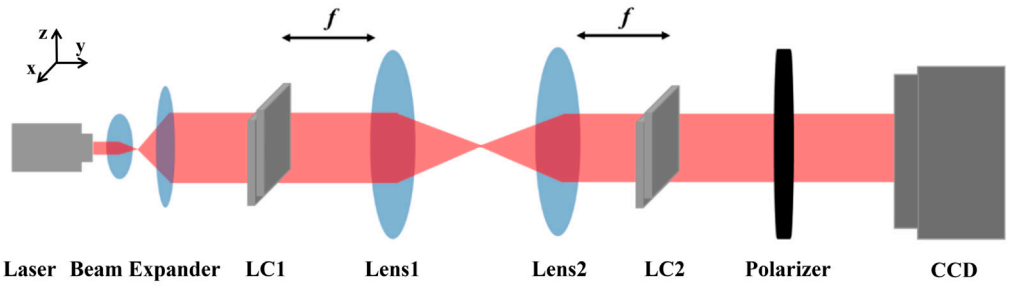


Figure 3. Schematic diagram of the optical path for the encryption with cascaded LC elements, where LC1 and LC2 are the encryption and decryption liquid crystal elements, respectively.

In Figure 2, only two LC directions (single image) were used, allowing more orientation error for LC molecules. If increasing the number of LC directions in the encryption, it will be more challenging to break the encryption through brute force, thereby improving the security of the information, but also requiring more LC directions.

To validate the above analysis, three images of "N", "P", and "U" were integrated into the encryption phase mask, and the corresponding three distinct decryption phase keys were generated. In the system, switching between different decryption phases allows for the display of varying information. This enables the adjustment of the outgoing light's phase using different decryption phases, while keeping the phase of the outgoing light through the encryption phase mask constant.

The experimental results are presented in Figure 4. The dark lines observed in the microscopic images are azimuthal defect lines formed at the boundaries between adjacent regions with different LC orientation angles. Microscopic photographs of the encrypted phase and decrypted phases were captured under crossed polarizers. Reconstructed images show clear NPU letters owing to the good alignment quality of LC molecules.

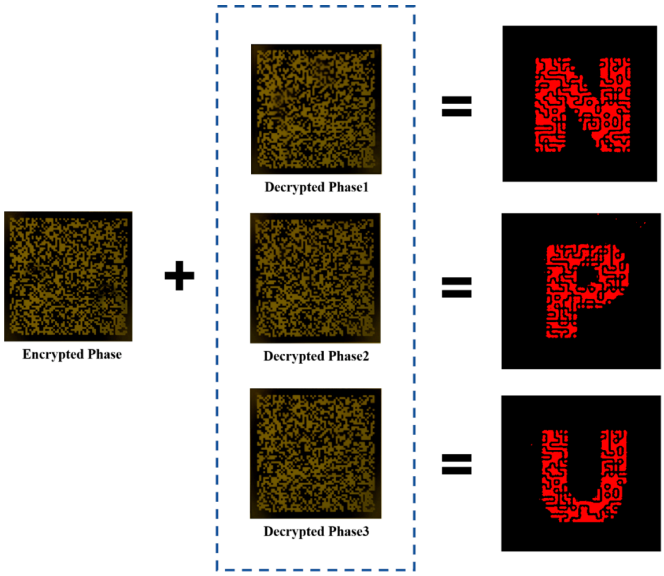


Figure 4. Microscopic photographs of the liquid crystal elements and the corresponding reconstructed images.

As shown in Figure 5, four binary images were stacked to generate an integrated image with 16 distinct grayscale values. The integrated image was then scrambled, resulting in an encryption phase matrix with 16 distinct phase values. Similarly, by combining the binary images before integration with the encryption phase matrix, the decryption phase also contains 16 different values, leading to distinct decryption phases. Compared with encryption using only two angles, multi-image integration offers higher security with more liquid crystal molecular orientations. As can be seen from the experimental results in Figure 5c, good decryption performance is still achieved.

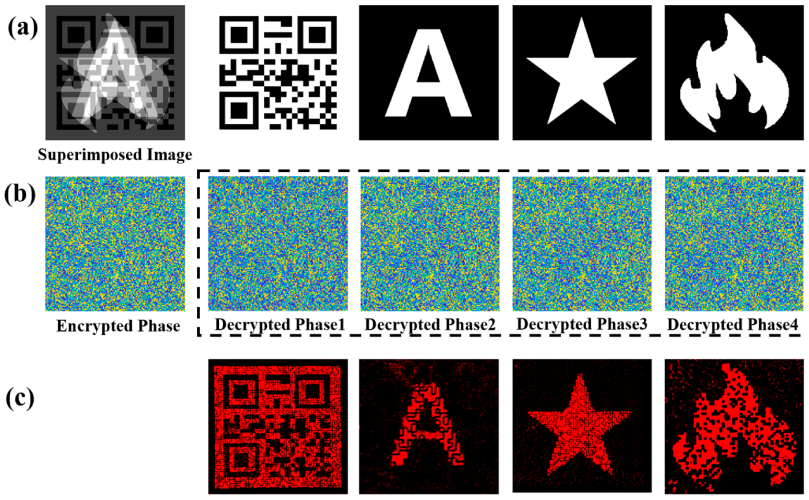


Figure 5. Schematic diagram of the multi-image integrated encryption principle: (**a**) integration of multiple two-gray-level images to form a mixed image; (**b**) generation of an encryption phase, and several decryption phases for target images; (**c**) experimental results of reconstructed images.

4. Security Analysis of the Encryption System

To further illustrate the safety of the proposed system, the vulnerability of the optical encryption scheme was tested with varying phase mismatch ratios and the alignment position of the LC elements. Figure 6 illustrates the effect of phase mismatch ratios on the quality of the decrypted image. The results reveal that when the mismatch ratio exceeds 10%, the decrypted image begins to blur. As the mismatch ratio increases, the image becomes more unidentifiable. When the mismatch ratio exceeds 20%, the "N" letter approaches the noise level and is nearly indistinguishable. After the mismatch ratio exceeding 30%, no valuable information can be recovered. This implies that an attacker, knowing the encryption phase matrix, must steal over 80% of the phase information from the decryption phase matrix to minimally recover the encrypted image.

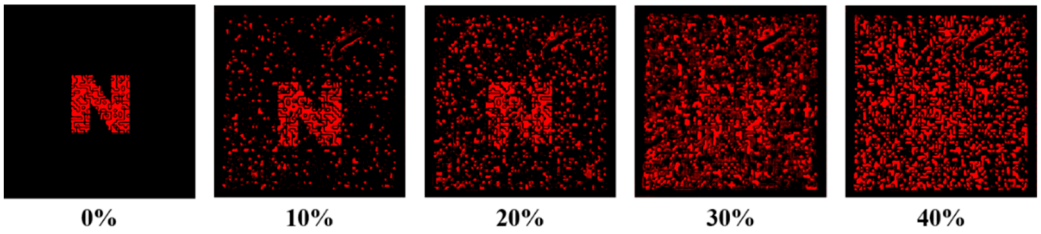


Figure 6. Decrypted images under different interference levels in the decryption phase.

Figures 7 and 8 illustrate the variation in decrypted image quality due to spatial misalignment. Figure 7 demonstrates the effect of lateral translation, where a displacement platform moves the decryption phase LC sample horizontally, with the imaging effect observed in real time. As the lateral misalignment between the LC elements increases, the quality of the decrypted image worsens. Given that the fabricated LC devices have a square region with the same LC molecular alignment vector of 0.105 mm × 0.105 mm and the total orientation pattern size is 7 mm × 7 mm. Therefore, any lateral misalignment greater than 0.105 mm theoretically causes complete misalignment of the two-phase matrices, preventing information retrieval. Experimental results show that when misalignment is larger than 0.08 mm, the letter N is almost unrecognized.

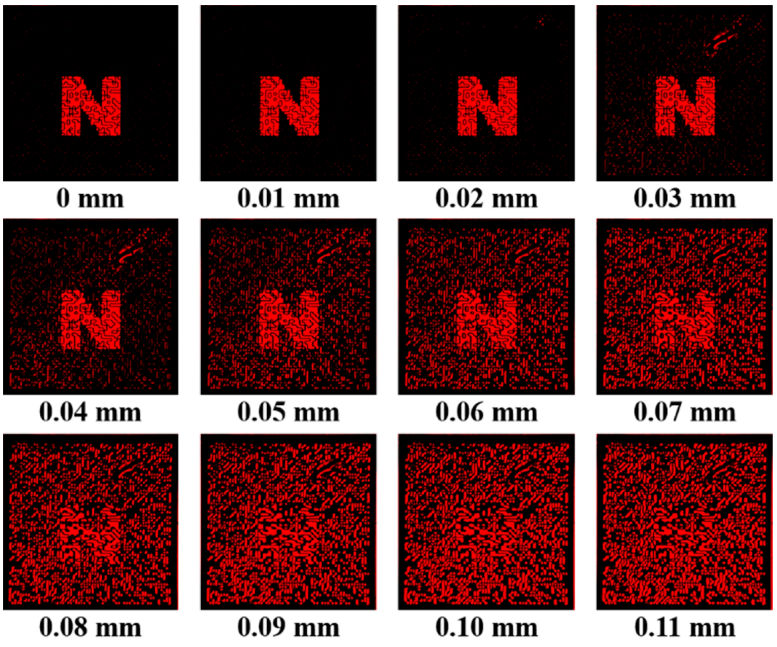


Figure 7. Decrypted images under different lateral translations.

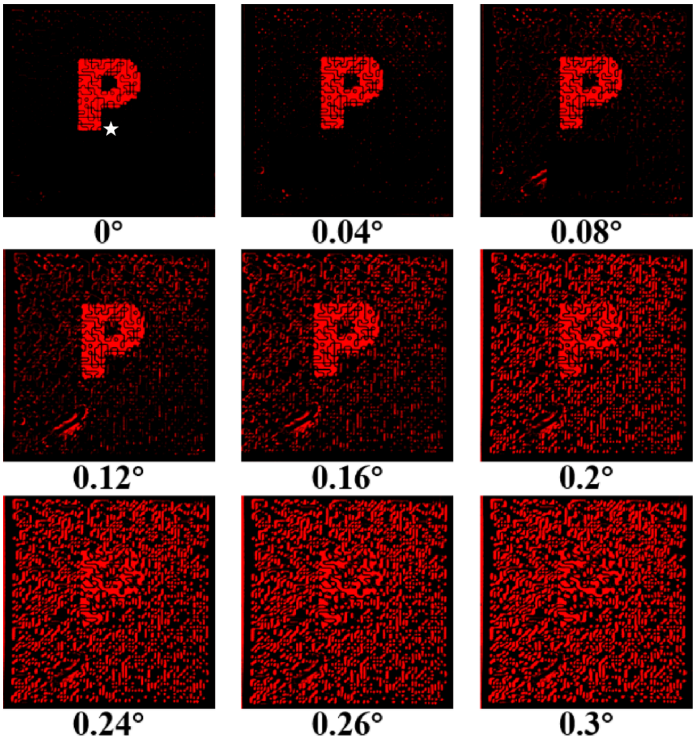


Figure 8. Decrypted images under different rotational misalignments, with the rotational center marked as a white star in the upper left photo.

Figure 8 illustrates the experimental results after rotating the two phases at different angles to induce misalignment. The white star marks the rotation center, about which all subsequent rotations are carried out. The quality of the decrypted image declines significantly as the rotation angle increases. When the rotational angle exceeds 0.2°, the decrypted image becomes unrecognizable. After the misalignment exceeds 0.3°, no usable information can be retrieved. Even slight lateral translations or rotations can cause the failure of image decryption. The decrypted image's sensitivity to position and angle further strengthens the security of optical encryption. Based on the above results, it is clear that lateral position searches must be precise to the micron level, while angle searches must be accurate to two decimal places. Thus, it is nearly impossible to identify if the speckle pattern is due to imperfect alignment or incorrect phase keys, making the system more vulnerable to brute-force attacks. The above analysis assumes the attacker is aware of the spatial misalignment and rotation angles of the two-phase matrices (which will be analyzed later). Without this information, the decryption time would be even longer.

To quantitatively analyze variations in image quality, the structural similarity index (SSIM) is employed to characterize the differences between decrypted images under mismatched conditions and those obtained under correct matching. SSIM is a perceptual metric used to evaluate the similarity between two images by comparing their luminance, contrast, and structural information. The SSIM value ranges from 0 to 1, where a value of 1 indicates perfect structural similarity. In general, SSIM values below 0.5 are considered to indicate significant structural differences, while values below 0.3 suggest severe distortion or a substantial loss of structural correspondence. As shown in Table 1, only when the lateral misalignment is less than 0.03 mm or the rotational misalignment is less than 0.04° does the decrypted image maintain a high degree of similarity to the correctly matched result. These results indicate that the system exhibits high sensitivity

to misalignment, which further demonstrates its high security and resistance to brute-force attacks.

Table 1. Structural similarity index under different mismatching conditions.

Type	Amplitude of Variation	SSIM
Phase Mismatch Ratio	10%	0.375
	20%	0.237
	30%	0.144
	40%	0.128
Lateral Displacement Misalignment	0.01 mm	0.976
	0.02 mm	0.909
	0.03 mm	0.669
	0.04 mm	0.319
	0.05 mm	0.254
	0.06 mm	0.170
	0.07 mm	0.155
	0.08 mm	0.127
	0.09 mm	0.111
	0.10 mm	0.104
	0.11 mm	0.093
Rotational Misalignment	0.04°	0.648
	0.08°	0.479
	0.12°	0.296
	0.16°	0.197
	0.2°	0.100
	0.24°	0.082
	0.26°	0.058
	0.3°	0.053

5. Conclusions

In summary, we have proposed and experimentally demonstrated an optical encryption method based on cascaded LC elements with multi-image integration. Depending on the number of integrated images, by designing 2 to 16 orientational angles of LC molecules, we fabricated several photo-aligned LC elements using our single-step exposure system. The LC elements used for encryption in this study were measured at only 7 mm × 7 mm. Experimental results show that when cascading LC elements in good position alignment, one to four images can be reconstructed in good quality. Future work can be done by using 32 or more distribution angles for 5 or more images. Furthermore, we also demonstrate that when the mismatch of the phases is greater than 20% or two LC elements have lateral and rotational misalignment greater than 0.08 mm and 0.2°, the reconstructed images are unrecognizable, showing good resistance to brute-force attacks. Our work suggests that the designed LC elements offer better image capacitance, along with the benefits of easy manufacturing, cost-effectiveness, and mature technology. With these advantages, the proposed cascaded LC scheme has great potential for future usage in optical encryption.

Author Contributions: Conceptualization, Y.M. and Y.C. (Yongning Cheng); methodology, Y.C. (Yongning Cheng) and H.L.; software, Y.C. (Yongning Cheng); validation, Y.M., H.L. and Y.C. (Yuechu Cheng); writing—review and editing, Y.M. and Y.C. (Yuechu Cheng). All authors have read and agreed to the published version of the manuscript.

Funding: This research was funded by the National Natural Science Foundation of China (NSFC) (62275220).

Institutional Review Board Statement: Not applicable.

Informed Consent Statement: Not applicable.

Data Availability Statement: Data are available from the authors on request.

Conflicts of Interest: The authors declare no conflicts of interest.

References

1. Chen, W.; Chen, X. Optical cryptography topology based on a three-dimensional particle-like distribution and diffractive imaging. *Opt. Express* **2011**, *19*, 9008–9019. [CrossRef] [PubMed]
2. Chen, W.; Javidi, B.; Chen, X. Advances in optical security systems. *Adv. Opt. Photon.* **2014**, *6*, 120–155. [CrossRef]
3. Refregier, P.; Javidi, B. Optical image encryption based on input plane and Fourier plane random encoding. *Opt. Lett.* **1995**, *20*, 767–769. [CrossRef] [PubMed]
4. Han, X.; Zhang, K.; Jin, W.; Zhu, W.; Li, Y.; Ma, L. Deep learning decryption approach for asymmetric computer-generated holography (CGH) cryptosystem. *Opt. Express* **2024**, *32*, 22249–22262. [CrossRef] [PubMed]
5. Chen, W.; Chen, X.; Sheppard, C.J.R. Optical color-image encryption and synthesis using coherent diffractive imaging in the Fresnel domain. *Opt. Express* **2012**, *20*, 3853–3865. [CrossRef] [PubMed]
6. Liu, W.; Liu, Z.; Liu, S. Optical security validation using Michelson interferometer. *Appl. Opt.* **2015**, *54*, 1802–1807. [CrossRef]
7. Jia, W.; Wen, F.J.; Chow, Y.T.; Zhou, C. Binary image encryption based on interference of two phase-only masks. *Appl. Opt.* **2012**, *51*, 5253–5258. [CrossRef] [PubMed]
8. Qu, G.; Yang, W.; Song, Q.; Liu, Y.; Qiu, C.-W.; Han, J.; Tsai, D.-P.; Xiao, S. Reprogrammable meta-hologram for optical encryption. *Nat. Commun.* **2020**, *11*, 5484. [CrossRef] [PubMed]
9. Zhang, X.; Ji, X.; Li, X.; Zhang, S.; Wang, H.; Li, J.; Li, X.; Wang, Y.; Huang, L. Spatial Varying Vectorial Holography and Polarization Encryption Based on Birefringent Metasurface. *Adv. Funct. Mater.* **2024**, *34*, 2404196. [CrossRef]
10. Zhu, S.; Dong, B.; Guo, G.; Lu, X.; Xu, Q.; Han, J.; Huang, W.; Ma, H.; Wang, Y.; Zhang, X.; et al. Terahertz Metasurfaces for Thermally Controlled Optical Encryption. *Laser Photonics Rev.* **2023**, *17*, 2300233. [CrossRef]
11. Kim, H.; Jung, J.; Shin, J. Bidirectional Vectorial Holography Using Bi-Layer Metasurfaces and Its Application to Optical Encryption. *Adv. Mater.* **2024**, *36*, 2406717. [CrossRef] [PubMed]
12. Sun, Y.; Geng, G.; Wang, Y.; Zhang, Y.; Li, Z.; Liu, W.; Cheng, H.; Chen, S. Multichannel Linear and Nonlinear Information Encryptions with Malus Metasurfaces. *Laser Photonics Rev.* **2024**, *18*, 2300866. [CrossRef]
13. Wei, Q.; Huang, L.; Zhao, R.; Geng, G.; Li, J.; Li, X.; Wang, Y. Rotational Multiplexing Method Based on Cascaded Metasurface Holography. *Adv. Opt. Mater.* **2022**, *10*, 2102166. [CrossRef]
14. Zhang, Z.; Yang, X.; Zhao, Y.; Ye, F.; Shang, L. Liquid Crystal Materials for Biomedical Applications. *Adv. Mater.* **2023**, *35*, 2300220. [CrossRef] [PubMed]
15. Peng, C.; Xu, C.; Hu, W. Smart beam via electrically addressing the dye-doped and polymer-stabilized cholesteric liquid crystals. *Chin. Opt. Lett.* **2024**, *22*, 053301.
16. Li, Y.; Liu, Y.; Li, S.; Zhou, P.; Zhan, T.; Chen, Q.; Su, Y.; Wu, S.-T. Single-exposure fabrication of tunable Pancharatnam-Berry devices using a dye-doped liquid crystal. *Opt. Express* **2019**, *27*, 9054–9060. [CrossRef] [PubMed]
17. Fu, W.; Zhou, Y.; Yuan, Y.; Lin, T.; Zhou, Y.; Zeng, T.; Huang, H.; Fan, F.; Wen, S. Symmetric Airy vortex and symmetric Airy vector beams. *Liq. Cryst.* **2021**, *48*, 484–490. [CrossRef]
18. Kim, J.; Li, Y.; Miskiewicz, M.; Oh, C.; Kudenov, M.; Escuti, M. Fabrication of ideal geometric-phase holograms with arbitrary wavefronts. *Optica* **2015**, *2*, 958–964. [CrossRef]
19. Xu, X.; Qiao, S.; Guo, Y.; Zhang, Q.; Fu, G.; Pu, M.; Fan, Y.; Li, X.; Zhang, F.; Xu, M.; et al. Optical Information Encryption Based on Secret Sharing Liquid Crystal Elements with Spatial Dislocation. *Laser Photonics Rev.* **2024**, *18*, 2400168. [CrossRef]
20. Tang, D.; Shao, Z.; Zhou, Y.; Lei, Y.; Chen, L.; Xie, J.; Zhang, X.; Xie, X.; Fan, F.; Liao, L.; et al. Simultaneous Surface Display and Holography Enabled by Flat Liquid Crystal Elements. *Laser Photonics Rev.* **2022**, *16*, 2100491. [CrossRef]
21. Xie, X.; Du, W.; Shao, Z.; Zhou, Y.; Lou, Z.; Ji, R.; Wen, D.; Wei, B.; Gan, X.; Zhao, J.; et al. Multichannel Binary-Image and Holographic Display Based on Planar Liquid Crystal Devices. *Laser Photonics Rev.* **2023**, *17*, 2300193. [CrossRef]
22. Tang, D.; Shao, Z.; Xie, X.; Zhou, Y.; Zhang, X.; Fan, F.; Wen, S. Flat multifunctional liquid crystal elements through multi-dimensional information multiplexing. *Opto-Electron. Adv.* **2023**, *6*, 220063. [CrossRef]
23. Chen, K.; Xu, C.; Zhou, Z.; Li, Z.; Chen, P.; Zheng, G.; Hu, W.; Lu, Y. Multifunctional Liquid Crystal Device for Grayscale Pattern Display and Holography with Tunable Spectral-Response. *Laser Photonics Rev.* **2022**, *16*, 2100591. [CrossRef]
24. Shi, Z.; Zheng, Z.; Wang, H.; Xu, X.; Li, X.; Zhang, Q.; Zhao, Q.; Shi, J.; Xu, M.; Zhang, F.; et al. Multi-Dimensional Multiplexing Cascaded Liquid Crystal Elements for Compartmentalized Optical Encryption. *Laser Photonics Rev.* **2026**, *20*, e03039. [CrossRef]

25. Wang, Z.; Zhang, H.; Liu, X.; Dou, Y.; Duan, W.; Chen, W.; Ma, L.; Lu, Y. Cascaded liquid crystal holography for optical encryption. *Chin. Opt. Lett.* **2023**, *21*, 120003. [CrossRef]
26. Ma, Y.; Yin, M.; Shan, Y.; Liu, X.; Qi, S.; Chigrinov, V.G.; Kwok, H.-S.; Zhao, J. Ferroelectric liquid crystal Pancharatnam-Berry lens with a fast control of output light's polarization-handedness. *Opt. Express* **2021**, *29*, 27472–27480. [CrossRef] [PubMed]

Disclaimer/Publisher's Note: The statements, opinions and data contained in all publications are solely those of the individual author(s) and contributor(s) and not of MDPI and/or the editor(s). MDPI and/or the editor(s) disclaim responsibility for any injury to people or property resulting from any ideas, methods, instructions or products referred to in the content.